Effect of sputtering pressure on the structure and current-perpendicular-to-the-plane magnetotransport of Co/Ag multilayered films

Wen-C. Chiang and W. P. Pratt, Jr.
Department of Physics and Astronomy, Center for Fundamental Materials Research, and Center for Sensor Materials, Michigan State University, East Lansing, Michigan 48824

M. Herrold and David V. Baxter
Department of Physics, Indiana University, Bloomington, Indiana 47405
(Received 9 March 1998)

Co/Ag multilayers have been sputter-deposited at pressures ranging from 0.86 to 10 mTorr, and magnetotransport measurements have been performed with the current both perpendicular to the plane (CPP) and in the plane (CIP) of the samples. X-ray-scattering studies indicate that the roughness of the interfaces is influenced by the presence of the Nb layers used to make electrical contact for the CPP measurements, as well as by the sputtering pressure. For samples deposited at higher sputtering pressures, the Nb contact layers also influence the low-temperature coercive field of the multilayers. The CPP-giant magnetoresistance is observed to decrease with increasing sputtering pressure and, in the case of the signal observed after cycling to above the saturation field, this decrease is found to come in roughly equal measure from an increase in the high field-saturated specific resistance and a decrease in the field-dependent specific resistance. Making use of the direct connection between microscopic physical parameters and experimental results available through the CPP geometry, we show that both of these changes arise primarily from increased scattering in both spin channels. We see very little, if any, evidence for a change in the spin-dependent scattering with sputtering pressure. [S0163-1829(98)03233-0]

I. INTRODUCTION

The giant magnetoresistance (GMR) effect, and the associated oscillatory exchange coupling of magnetic layers across nonmagnetic spacer materials in magnetic multilayers,[1,2] continue to be of great interest at both a fundamental level and for technological application. While it is widely accepted that GMR arises from spin-dependent scattering,[3] the actual mechanism responsible for the spin dependence remains unclear. This is particularly true for the interfaces, where most of the spin-dependent scattering events relevant to practical devices are thought to occur. Numerous investigations have been undertaken to explore the relationship between interfacial structure and GMR over the past several years to address this issue. These have included studies where the interface was altered by growing films with different deposition conditions (such as growth temperature, sputtering pressure, etc.),[4–7] through deposition of an interfacial layer,[8,9] or through annealing.[10,11] Studies have been performed on a variety of different systems, but most have concentrated on either Fe/Cr (Refs. 5, 7, 12, and 13) or Co/Cu.[9,11,14]

The role of interfacial structure on the CIP-GMR has also been studied in Co/Ag multilayers recently by other researchers[11,19] who altered the interfacial structure through low-temperature annealing. Anneals near 350 °C were found to increase the GMR signal by a factor of 2 or 3, but there is as yet no consensus as to the structural changes responsible for this increase. This temperature is comparable to that found to produce an enhanced GMR through the formation of a discontinuous structure in the magnetic layers of NiFe/Ag multilayers,[20] but no confirmation of the same behavior arising in the Co/Ag system has been published. In the present study, results from the CPP geometry are correlated with changes in the atomic structure as determined from x-ray scattering. Although it has not been as extensively studied, the Co/Ag system shares with the Co/Cu system the advantage of having immiscible constituents but offers better x-ray contrast. This makes Co/Ag attractive for looking at the connection between structure and transport properties.

At least three significant complications must be confronted in trying to relate changes in interfacial structure to changes in transport properties in GMR materials. First, it is difficult to quantify the nature of the structural defects incorporated into the multilayer via the various procedures mentioned above. Not only the overall ''roughness'' but also the length scales over which correlations persist (both laterally, along each interface, and vertically, from one interface to the next) can be important. Unfortunately, a complete characterization of the roughness of buried interfaces is not possible with present techniques. Off-specular x-ray scattering and NMR hold promise for providing some useful information in this regard,[15–18] but even these techniques have not always been employed. Second, it is also difficult to relate changes in interfacial structure directly to the transport properties in the traditional transport geometry where the current is in the sample plane (the so-called CIP geometry). Finally, in samples with thin nonmagnetic layers, one must distinguish the direct effects of structural changes on the transport properties from concomitant changes they may be induced on the interlayer coupling. An indication of the impact of these complications may be seen in the conflicting results obtained in published studies.[5,10,14]

0163-1829/98/58(9)/5602(9)/$15.00 © 1998 The American Physical Society

Some of the difficulties discussed above may be overcome by studying the magnetotransport of multilayers with thick nonmagnetic layers (to reduce effects from changes in the interlayer coupling) and by using the current-perpendicular-to-the-planes (CPP) geometry. This paper presents results from a study of the relationship between the CPP-GMR and interfacial roughness in multilayers. We study Co/Ag multilayers with Ag layers sufficiently thick to decouple the Co layers. The structure of the samples was altered by growing films under various Ar sputtering pressures and this structure was studied using both specular and diffuse x-ray scattering. Using the unique advantages of the CPP measurement geometry, we are able to show that the observed decrease in the magnetoresistance (MR) with increasing sputtering pressure for these samples is due to an overall increase of the scattering in both spin channels rather than a change in the spin-dependent scattering.

II. EXPERIMENT

The Co/Ag multilayers were made by sputtering in an ultrahigh-vacuum compatible, four-target system, using preparation conditions and procedures described elsewhere.[21] The sputtering system was initially pumped down to $\sim 2 \times 10^{-8}$ Torr. High-purity Ar sputtering gas was then admitted and the sputtering pressure (P_{sputt}) was set. The multilayers were designed to have thicknesses $t_{\mathrm{Co}} = 3$ nm and $t_{\mathrm{Ag}} = 8$ nm with 10 bilayers in each sample. An extra Co cap layer (3 nm in thickness) was included to suppress proximity-induced superconductivity from the Nb leads used for the CPP measurement. The Ag layer thickness should be large enough to effectively decouple the magnetic layers.[22] The samples make use of a geometry in which the CIP and CPP transport properties may be measured simultaneously. Details regarding their geometry and fabrication, including the *in situ* mask-changing system, which makes the CPP geometry possible, are discussed at length in previous publications.[21–23] For the present discussion it is important to note that the CPP measurements are made on a central portion of the multilayer sandwiched between a pair of crossed Nb strips (one below, the other above). The Nb strips are approximately 1.1 mm wide and 250 nm thick and serve as both current and voltage leads. To avoid shorts between the Nb strips and minimize the influence of the Nb on the CIP measurement, the Co/Ag multilayers have a circular central region (roughly 4 mm in diameter) where the Nb strips cross. Two narrower strips of the multilayer bring the CIP current into and out of this circular region and these narrower strips therefore dominate the CIP measurement. With this configuration the CIP current geometry is not precisely controlled, and consequently greater sample-to-sample variation is seen in the CIP measurements than in the CPP measurements.

Several series of samples with the same nominal structure were deposited onto Si(001) substrates at Ar sputtering pressures of 0.86, 1.3, 2.5, 5.5, and 10 mTorr (as read by a Bayard-Alpert ion gauge operating at 0.1 mA emission current). Samples deposited on sapphire substrates showed qualitatively similar transport properties (though typically with a weaker dependence on sputtering pressure) but the sapphire substrates were not suitable for x-ray characterization, so those samples are not included in the discussion below. The sputtering power applied to each target was held constant and the resulting rates at the given pressures were 4.2, 3.9, 3.6, 2.6, and 1.4 Å/s, respectively, for Co, and 10.7, 10.5, 9.8, 7.4, and 4.6 Å/s, respectively, for Ag as measured by quartz crystal monitors. The substrates were held at a distance of 12 cm from the sources. The Nb strips for all samples were made at 2.5 mTorr of Ar, at a rate of ~6 Å/s. The Nb leads on the transport samples make them ill-suited for structural characterization, so in the same deposition run, and under identical conditions, unpatterned multilayers were made on $12 \times 12\ \mathrm{mm}^2$ substrates for the x-ray-diffraction measurements. These ''x-ray samples'' were made with a 250 nm Nb buffer layer between the Co/Ag multilayer and the substrate, and the extra 3 nm Co cap layer, but without the top Nb layer. Later, in separate runs under nominally identical conditions, similar x-ray samples were made without the Nb buffer layer in order to investigate the influence of this layer on the structure of the multilayer.

A reference resistor and SQUID-based system are used to measure the CPP magnetoresistance. At the measuring temperature of 4.2 K, the Nb strips superconduct, becoming equipotential contacts, thereby ensuring that a uniform current density (of roughly 8 $\mathrm{A/cm}^2$) passes through the overlap area ($A \sim 1.25\ \mathrm{mm}^2$) between the strips. The CPP geometry allows the measurement of the specific resistance AR, the product of the overlap area of the Nb strips and the resistance through the multilayer. The cross-sectional area of the CPP sample, A, was measured by a Dektak profilometer. Further details have been provided in an earlier publication.[22]

X-ray diffraction was performed on a Scintag XDS2000 horizontal θ-2θ diffractometer, using Cu $K\alpha$ radiation from a sealed line-focus tube. A Ni filter on the incident beam and liquid-nitrogen-cooled Ge detector were used to eliminate the $K\beta$ radiation. The incident beam had a horizontal divergence of 0.07° and the detector slit had a horizontal acceptance of 0.28° and a vertical acceptance of 4.8°. The large vertical acceptance means that the data collected are integrated over one of the lateral directions in reciprocal space and thereby allow the interpretation of the scattering in terms of a single lateral direction. For scattering angles (2θ) less than 1.5° the intensity from the x-ray tube was reduced by a factor of 400 by decreasing the power from 40 kV and 35 mA to 12 kV and 2 mA.

III. RESULTS AND DISCUSSION

A. Structural characterization

Representative low-angle x-ray patterns are shown in Fig. 1. This figure shows data collected in the specular θ-2θ mode (continuous curves) along with data collected with ω (the incident angle of the x rays with respect to the sample surface) offset by 0.2° from the specular condition (dot-dashed curves). Data collected in the latter mode probe the diffuse intensity along a cut through reciprocal space almost parallel to q_z (the growth direction of the multilayer). If this intensity exhibits maxima when q_z lies on the Bragg planes in reciprocal space, the roughness has some correlation from one interface to the next.[15,24] The data in Fig. 1 have been normalized to the incident intensity and have been corrected for detector dead time and for the finite sample size, which causes some of the beam to miss the sample at the lowest

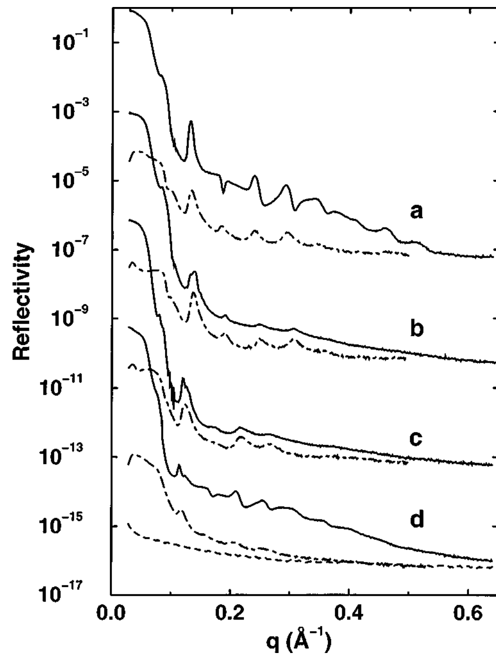

FIG. 1. Low-angle x-ray-scattering results for representative samples deposited on Si under various sputtering pressures. The continuous curves display the specular data while the dot-dashed curves show the data collected with the incident angle (ω) offset from the specular condition by 0.2°. Curves a and d are from samples prepared without a Nb buffer layer at 2.5 and 10 mTorr, respectively, while b and c are from samples prepared with a Nb buffer layer at 2.5 and 10 mTorr, respectively. The successive pairs of curves have been displaced by a factor of 10^{-3} for clarity of presentation. The dashed curve at the bottom of the graph shows the contribution from air scattering (on the same scale as curve d).

angles (''footprint'' correction). Uncertainties in these corrections and in the value of the incident intensity, along with possible deviations of the sample surface from a plane over macroscopic length scales (i.e., figure error), could introduce a systematic error in the reflectivity of up to 15%. In no case would the conclusions drawn below be altered by a systematic error of this magnitude.

The modulation wavelength for each sample may be found by fitting the observed specular scattering peak positions to Bragg's law with the inclusion of the refraction correction.[25] The resulting values for the modulation wavelengths of the samples are shown in Table I. Independent of the presence of the Nb buffer layer, the samples prepared at pressures below 10 mTorr have modulation wavelengths within 5% of each other (and clustered within 5% of the nominal value of 110 Å), while the samples prepared at 10 mTorr have periods 10–15 % above the nominal value. Since t_{Ag} is large enough to decouple the Co layers, this slight difference in modulation wavelength is not expected to affect the magnetoresistance significantly.

Two other trends are also immediately apparent from the data displayed in Fig. 1. The samples prepared without the Nb buffer layer show a better-defined diffraction pattern and a greater intensity difference between the specular and offset scans than in those prepared with a Nb buffer layer. The samples prepared at higher sputtering pressures also display less structure in their diffraction pattern than do samples prepared at lower pressures. This latter trend is consistent with results seen in other systems, and indicates that the samples prepared at higher pressures are rougher.[7,12] Earlier work on other systems indicates that both topographic roughness (step edges) and chemical disorder (intermixing of Co and Ag) increase with sputtering pressure[12] and similar behavior is expected for the present samples. The marked difference in the x-ray pattern that accompanies the introduction of the Nb (e.g., compare curve a with b, or c with d, in Fig. 1) indicates that this buffer layer is quite rough and its presence significantly increases the overall roughness of these multilayers. The roughness introduced at the interfaces of the multilayer as a result of growth on this rough buffer layer should be dominated by topographic rather than chemical disorder.

As a result of the roughness introduced by the Nb buffer, structural changes associated with different sputtering pressures are most easily seen in the samples made without buffer layers. This is shown most dramatically in Fig. 2, where we have plotted the measured crystalline coherence length (ξ) vs sputtering pressure for samples grown on Si (both with and without Nb buffer layers). The value of ξ was determined from the width of the superlattice peaks seen at high angles using the Scherrer formula[26] and therefore represents lattice coherence in the growth direction. While both sets of samples exhibit shorter coherence lengths at the larger sputtering pressure, the trend is much more pronounced in

TABLE I. Structure and CIP-transport characterization of Co/Ag multilayers (the ''x-ray samples'') produced at various sputtering pressures. ρ_m and R_m refer to the properties of the multilayer alone, having accounted for the contribution from the Nb buffer layer when it is present. Λ and σ_c are expressed in Å, and the resistivity is expressed in $\mu\Omega$ cm. All quoted transport values are based on measurements performed in a field of 1.2 kOe and thus should be correlated with the atomic structure, not the magnetic structure, of the multilayer.

P_{sputt} (mTorr)	Buffer	Λ ($\pm$1 Å)	$\frac{R\,(200\text{ K})}{R\,(12\text{ K})}\pm 1\%$	$\frac{R_m\,(200\text{ K})}{R_m\,(12\text{ K})}$	ρ_m (12 K) ($\mu\Omega$ cm)	σ_c ($\pm$0.3 Å)
0.86	None	106.6	1.31	1.31± 1%	11.4±10%	0.8
2.5	none	112.0	1.41	1.41± 1%	6.8±10%	1.3
5.5	none	113.4	1.24	1.24± 1%	17.6±10%	1.4
10.0	none	125.9	1.20	1.20± 1%	14.5±10%	1.4
0.86	Nb	104.6	1.96	1.13±10%	9.8±15%	2.5
2.5	Nb	106.2	2.11	1.70±10%	4.7±15%	4.6
5.5	Nb	106.9	1.88	1.03±10%	9.1±15%	3.8
10.0	Nb	120.2	1.92	1.33±10%	5.0±15%	3.9

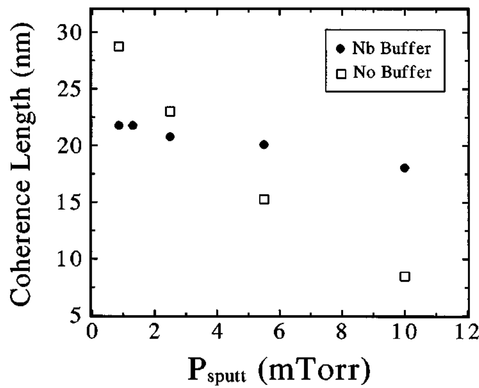

FIG. 2. Crystalline coherence length (ξ) (as determined from peak widths in high-angle x-ray diffraction using the Scherrer equation) for Co/Ag samples deposited on Si under various sputtering pressures. The variation of ξ with pressure is much stronger in samples prepared without a Nb buffer layer.

the samples without the buffer layer. It is interesting to note that ξ is not linked in any simple way with the overall interfacial disorder since samples grown on the rough buffer layer exhibit a shorter coherence length at low pressures, but a longer coherence length at high pressures, than samples grown directly on Si. The sputtering pressure dependence of ξ must therefore reflect a compromise between the competing influences of the incident atom energy (which varies with sputtering pressure) and substrate roughness on the structure of the growing film. This appears to be a subject worth further investigation.

The nature of the disorder at the interfaces in these samples determines the distribution of diffuse x-ray scattering in reciprocal space. Unfortunately, a complete quantitative analysis of the diffuse scattering from multilayers is not yet possible due to complications from dynamical scattering effects and the need for accurate modeling of both the instrumental resolution function and the disorder in the sample.[24,27] On the other hand, a number of authors have pointed out recently that qualitative (and in some cases semiquantitative) information regarding the correlations exhibited by the disorder may be obtained from this diffuse scattering.[15,24,28] For instance, the offset scattering shown in Fig. 1 exhibits a trend similar to that discussed above for the crystalline coherence length. For the samples grown on Si without the Nb layer, the off-specular scattering is more homogeneous (indicating weaker vertical correlations in the roughness) at the higher sputtering pressure. The same behavior is seen for samples with the Nb buffer but in this series the dependence on sputtering pressure is much weaker (as can be seen most easily by comparing the offset data for curves *c* and *d* in Fig. 1). These observations are consistent with a view that increasing the sputtering pressure leads to rougher film growth and this, in turn, reduces the vertical correlations between the interfaces in the multilayer.

Correlations along each interface may be probed by looking along a direction perpendicular to the growth axis in reciprocal space. This is done, to a good approximation, by performing rocking curve measurements in which the scattering angle is kept fixed (at 2θ) while the incident angle (ω) is varied from 0 to 2θ.[15,24] Figure 3 shows rocking curves at the second-order peak for samples grown at four different

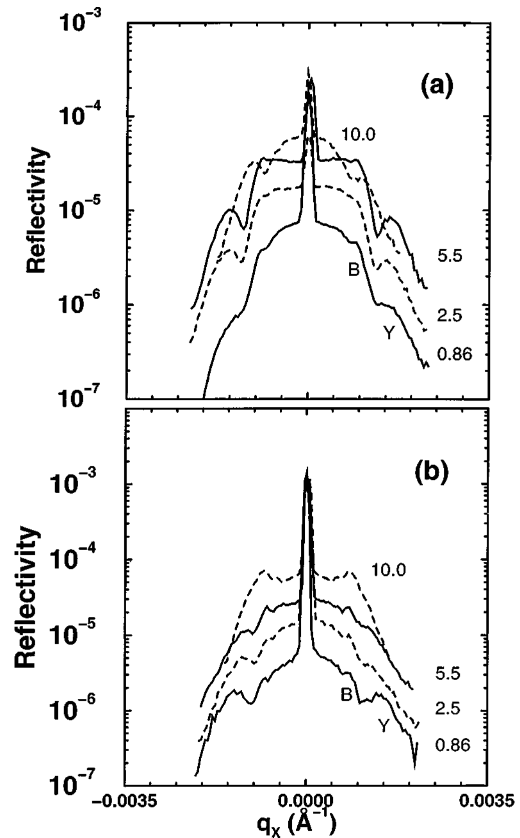

FIG. 3. Rocking curves at the second-order maximum for representative samples grown (a) with a Nb buffer layer and (b) without a Nb buffer layer. The number beside each curve gives the sputtering pressure used for producing that sample (in mTorr). The *Y* indicates the approximate position of the Yoneda peak, which arises when either the incident or outgoing angle equals the critical angle for external reflection, and the *B* indicates the Bragg-like multiple-scattering peak, which arises when the incident or outgoing angle is equal to the Bragg angle for the first-order peak. Successive curves have been multiplied by 2.5 to offset the diffuse scattering for clarity.

sputtering pressures with and without the Nb buffer layer. In this figure the data have been corrected for variations in the effective scattering volume as ω is varied[15] as well as the corrections applied to the data shown in Fig. 1. The most obvious feature in these data is that the central coherent scattering peak is more intense (both in absolute terms and relative to the diffuse background) in the samples grown without a Nb buffer layer than it is for those grown with the buffer layer. Savage *et al.* have suggested that the amount of roughness that is correlated from one interface to the next may be determined from the ratio of the integrated intensity under this coherent peak to the diffuse scattering integrated intensity.[15] The vertically correlated roughness may be computed as

$$\sigma_{\mathrm{corr}}=\frac{[\ln(r_c+1)]^{1/2}}{q_z}, \tag{3.1}$$

where q_z is the momentum transfer at which the rocking curve was taken and r_c is the ratio of the integrated diffuse intensity to the specular integrated intensity in the rocking curve:

$$r_c = \frac{\int I_{\mathrm{diff}} d\omega}{\int I_{\mathrm{spec}} d\omega}. \tag{3.2}$$

This interpretation is somewhat naive since some vertical correlation is automatically imposed by the periodic structure,[24] and the level of correlation in the vertical direction will be different for different lateral spatial frequencies.[29] Such measurements are also subject to systematic errors introduced by multiple scattering effects (such as those leading to the small ''Bragg-like'' peaks[30] seen inside the Yoneda peaks in Fig. 3).

With these qualifications in mind, the above procedure can nevertheless provide useful insight into the evolution of vertical correlations within a series of samples. The last column in Table I gives the average values for the correlated roughness as determined from Eqs. (3.1) and (3.2). From these numbers we can reach two conclusions. First, there is more vertically correlated roughness in samples with Nb buffer layers than in those grown directly on Si. The numbers for σ_c in Table I thus give a quantitative description of the strength of the coherent peak relative to the background (discussed qualitatively above). There is a small maximum in the value of the correlated roughness at a sputtering pressure of 2.5 mTorr. A similar small maximum is seen in the residual resistivity ratio, as seen in the fourth column of the table. Thus, growth at 2.5 mTorr provides a slightly more ordered sample than growth at other pressures, and some of this increased order appears as enhanced vertical correlations among the interfaces. The correlated roughness in the samples grown without the Nb buffer layer is small enough that this maximum cannot be seen over the noise in σ_c but it is visible in the residual resistivity ratio for these samples.

A somewhat more subtle dependence on sputtering pressure can be seen in the diffuse scattering in Fig. 3. This consists of a broadband of diffuse scattering under each coherent peak along with a pair of Yoneda peaks (one near both extremes of each scan produced by a standing wave enhancement when either the incident or outgoing angle equals the critical angle).[31,32] For some scans one can also see a weaker set of ''Bragg-like''[30] peaks arising from multiple scattering when either θ_{in} or θ_{out} is equal to the Bragg angle for a coherent peak in the specular scan. For the samples with the buffer layer, there is a well-defined plateau between the Yoneda peaks that flattens out as the pressure is increased and eventually rounds out as the pressure reaches 10 mTorr. The presence of this plateau and its variation with pressure indicate that much of the increased roughness introduced by the buffer layer is replicated from layer to layer during growth, but this replication becomes less precise as the pressure is increased. For the samples without the buffer layer the multilayer grows on a much smoother surface and there is less roughness to be carried throughout the structure so this feature is correspondingly weaker. Note that, independent of the presence of a buffer layer, the width of the diffuse scattering broadens as the sputtering pressure is increased. This width is inversely related to the width of the lateral correlation function for that part of the roughness that is correlated from one interface to the next. Within the model of self-affine structures commonly used to describe such interfaces, this latter width can be reduced either by shortening the lateral correlation length or through a reduction of the roughness exponent.[33] We are unable to distinguish between these two possibilities on the basis of the present data.

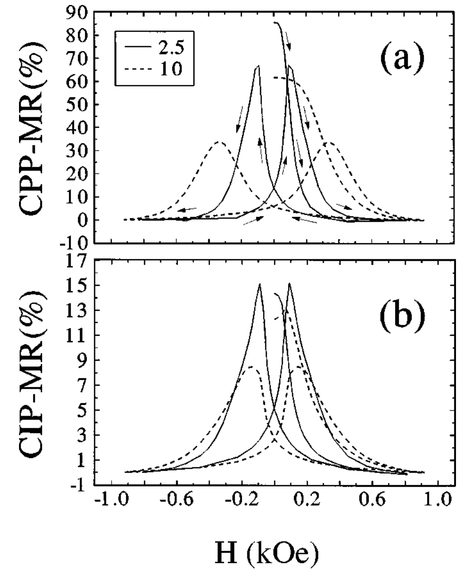

FIG. 4. MR curves, measured at 4.2 K, for samples with the structure $[\mathrm{Co}(3\,\mathrm{nm})/\mathrm{Ag}(8\,\mathrm{nm})]_{10}$ deposited on Si(001). The solid curve represents a sample deposited at 2.5 mTorr while the dashed curve is for a sample deposited at 10 mTorr. (a) displays data taken in the CPP geometry while (b) displays data collected in the CIP geometry. Note that MR is defined differently for CPP and CIP [see Eqs. (3.3) and (3.4)].

The primary features seen in the variation of the structure with sputtering pressure in these samples may be summarized as follows. The Nb buffer layer introduces a large amount of roughness, which imposes significant vertical correlations between the disorder at the interfaces in these multilayers. As the sputtering pressure is increased, the growth of the multilayer itself becomes rougher, reducing the strength of these vertical correlations. This increased disorder is also evident in the monotonic decrease in the crystalline coherence length with sputtering pressure. A more subtle effect is a small maximum in the overall order for the multilayers grown at 2.5 mTorr. This extremum is detected as a maximum in the residual resistivity ratio and is also visible in the average vertically correlated portion of the interfacial roughness for samples grown on Nb buffer layers.

B. Magnetotransport

Figure 4 shows both the CPP and CIP MR curves (measured at 4.2 K) for two samples, deposited at 2.5 and 10 mTorr, respectively, on Si(001) substrates. Here MR(H) is defined as

$$\mathrm{MR}(H) = \frac{[AR(H) - AR(H_S)]}{[AR(H_S) - 2AR_b]}\ (\%) \tag{3.3}$$

for CPP, and

$$\mathrm{MR}(H) = \frac{[R(H) - R(H_S)]}{R(H_S)}\ (\%) \tag{3.4}$$

for CIP. H is the applied magnetic field, H_S is the field at which the resistance saturates, $A \sim 1.25\ \mathrm{mm}^2$ (the overlap

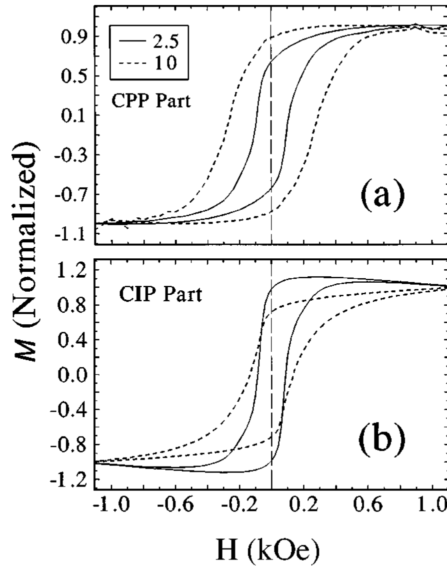

FIG. 5. Magnetization as a function of magnetic field, measured at 12 K, for two multilayers (deposited at 2.5 and 10 mTorr). (a) and (b) displays data taken using the CPP and CIP part of the sample, respectively (see text). The behavior at high fields in the measurement of the CIP part of the sample grown at 2.5 mTorr probably is the result of the diamagnetic signal from the substrate and is not of importance to the present study.

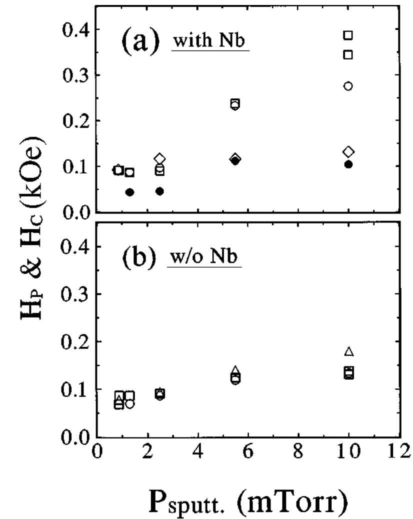

FIG. 6. Magnetic field scale vs sputtering pressure for various samples deposited on Nb buffer layers (a), and directly on Si (b). It is observed that a marked sputtering pressure dependence of the field scale arises only for those samples with Nb contact layers on both sides of the multilayer, and even then this dependence appears only at low temperatures. Open symbols represent data collected at low temperatures (with the precise temperature chosen according to whether the Nb layers needed to be normal or superconducting for the measurement), and the closed symbols show data collected at 300 K. □, H_P at 4.2 K; ○, H_C at 12 K; △, H_C at 5 K; ●, H_C at 300 K; ◇, H_C at 12 K. In (a) all samples have a Nb buffer layer, and all except those represented by the ◇'s also have an additional Nb overlayer. H_P refers to the position of the peak in the MR curve (see Fig. 4), whereas H_C refers to the coercive field measured in a direct measurement of the magnetization.

area between the two Nb strips), and $2AR_b = 6.1$ fΩ m^2 is the sum of the two CPP boundary resistances between Co and the superconducting Nb (a quantity that has been measured previously[22]). Looking at the figure, it is possible to define two different magnetoresistance ratios: MR(H_0) denoting the magnetoresistance referenced to the virgin state in which the sample was initially prepared with $H=0$, and MR(H_P) for the magnetoresistance referenced to the "peak" state at $H=H_P$, the field at which the resistance is maximum after cycling to above H_S. As seen in Fig. 4, both the magnitude and the shape of the MR curves are sensitive to changes in the sputtering pressure for both the CPP and CIP geometries. The change in shape is most easily characterized as changes in the value of H_P.

The most striking feature in Fig. 4 is the difference in the dependence of H_P on the sputtering pressure for the two current configurations. In an attempt to understand this difference, the magnetization was also measured as a function of magnetic field. Representative examples of these data are shown in Fig. 5. This figure shows the stabilized magnetization (M) curves, measured at 12 K, for samples produced at 2.5 and 10 mTorr. For these measurements no initial H_0 state could be recorded since the samples had previously been exposed to external fields in the MR measurements. To make direct comparison with the CPP-MR data possible, the central square of the CPP samples (that portion sandwiched between the Nb contact layers) was cut out from the patterned samples after all transport measurements were made, and the magnetization of only this ~ 1.25 mm^2 section was measured [Fig. 5(a)]. Comparison of the MR(H) and $M(H)$ curves shows that the hysteresis cycles follow each other closely, and the position of the peak in the MR approximately coincides with the coercive field (H_C). The increase in the coercive field with P_{sputt} is evident in the wider hysteresis loops seen for the 10 mTorr sample in Fig. 5(a). The remaining parts of the patterned samples (i.e., those portions without the Nb buffer and overlayer) were also measured and the resulting data are shown in Fig. 5(b). The data in Fig. 5(b) thus represent that part of the sample that dominates the MR measured in the CIP configuration, and they confirm the much reduced sputtering pressure dependence for the coercive field in this case.

Figure 6 shows the variation with sputtering pressure of both the H_P values determined from the magnetotransport and the coercive fields (H_C) determined from magnetization measurements. The figure confirms the strong correlation between H_P and H_C, and also makes evident the distinct difference between the samples used for the CPP and CIP measurements. This phenomenon is not simply associated with the growth processes on the Nb buffer. Samples grown on a Nb buffer layer, but with no overlayer (i.e., pieces taken from the corresponding Nb-buffered "x-ray samples") exhibit a coercive field that is essentially independent of sputtering pressure and comparable to that found in samples without the buffer layer. Moreover, a marked dependence of H_C (or H_P) on sputtering pressure is seen only in measurements made at low temperatures on multilayers sandwiched between Nb layers [see the ○ and □ symbols in Fig. 6(a)]. In contrast to this, when these same samples are measured at 300 K [filled circles in Fig. 6(a)], the coercive field is essentially indistinguishable from the measurements of H_P and H_C on samples without the two Nb layers (or those with only

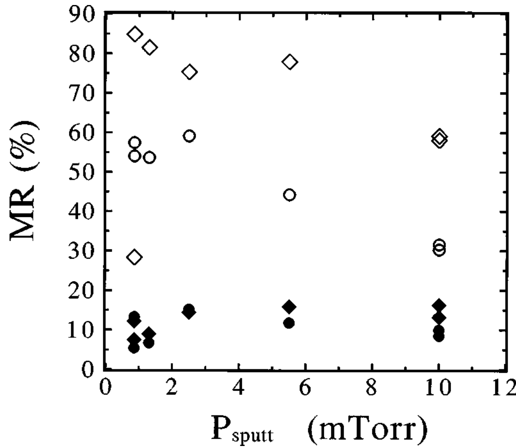

FIG. 7. Magnetoresistance ratio as a function of sputtering pressure for measurements in the CPP (open symbols) and CIP (closed symbols) geometries. Diamonds show MR(H_0) and circles show MR(H_P). In all cases the symbols provide an upper bound on the uncertainty in the measurement itself, while the scatter gives an indication of the variation from sample to sample. The larger relative size of the percent scatter in the CIP geometry and virgin state CPP data is discussed in the text.

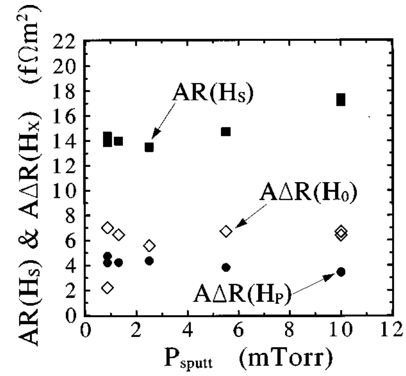

FIG. 8. The field-saturated specific resistance $AR(H_S)$ and field-dependent specific resistance $A\Delta R(H_x)$ (for both the virgin and "peak" states) measured in the CPP geometry at 4.2 K for Co/Ag multilayers deposited at various sputtering pressures.

the buffer layer). This indicates that the difference between the behavior of H_P in the CPP and CIP measurements arises from thermally induced stress imposed by the two Nb layers as the sample temperature is lowered. As discussed in the preceding section, the samples prepared at higher pressures are more disordered and hence more susceptible to stress-induced changes in their magnetic properties.

The CPP and CIP MR are plotted as a function of the sputtering pressure in Fig. 7 as open and closed points, respectively. The MR is plotted for both the virgin state [i.e., MR(H_0)] and the "peak" state [MR(H_P)]. In all cases the relative uncertainty in the measurement of the MR itself is on the order of 5% (the size of the symbols in the figure) or less, but the data show greater sample-to-sample variation than can be accounted for by this. For the CIP measurements, a possible origin of the variation from sample to sample is slight shifts of the substrate under the mask as the samples are shuttled from one source to the other during growth of the multilayer. Since the CPP measurement probes only the central section of a larger circular multilayer sample,[22] it is much less susceptible to such shifts than is the CIP measurement (see Fig. 7). As a result, with the exception of one of the 0.86 mTorr samples in the virgin state, the CPP measurements show significantly less percent scatter than do the CIP measurements. For this reason in the following we concentrate on the CPP results. Previous work[34] has indicated that the virgin state typically provides the best approximation to an antiparallel alignment of the magnetic layers in samples such as these (where the magnetic layers are uncoupled). The steady-state behavior (after cycling to fields above H_S) is quite similar for both 0.86 mTorr samples (see Fig. 8), so we attribute the anomalous CPP-MR(H_0) point to an unexpectedly small antiparallel fraction in the virgin state for the CPP section of one of the samples. In general, within this series of samples, the CPP-MR(H_0) is larger but exhibits more scatter from sample to sample than does the CPP-MR(H_P).

Although it is a quantity of considerable technological interest, the MR ratio itself is not the most useful quantity to study when trying to understand the relationship between structure and transport since it is sensitive to both the field-dependent resistance [the numerator in Eqs. (3.3) and (3.4)] and the resistance at H_S (the denominator in the same equations). To distinguish between these two dependences, we plot in Fig. 8 the field-dependent and field-saturated specific resistance values for the CPP measurements [i.e., $A\Delta R(H_x)=AR(H_x)-AR(H_S)$ and $AR(H_S)$ with H_x representing either H_P or H_0]. Figure 8 demonstrates that small, but measurable, changes occur in both $AR(H_S)$ and $A\Delta R(H_P)$ with changing sputtering pressure. The scatter in the $A\Delta R(H_0)$ data is too large to draw any conclusions on its variation with sputtering pressure. Once again in this figure the symbols provide upper bounds on the size in the uncertainty of the measurement itself while the scatter indicates the sample-to-sample variation. From Fig. 8 we see that the (roughly 45%) decrease of the MR(H_P) signal with increasing pressure arises in roughly equal measure from a (20±5%) decrease in $A\Delta R(H_P)$ and a (24±5%) increase in $AR(H_S)$.

Unfortunately $A\Delta R(H_x)$ and $AR(H_S)$ each depend on both spin-dependent and spin-independent scattering so this simple breakdown of the changes in MR does not shed direct light on the impact of structure on spin-dependent scattering. On the other hand, unlike CIP measurements, with CPP studies it is possible to construct a quantity that depends directly on the spin-dependent contribution:[22]

$$\sqrt{A\Delta R(H_x)\times AR(H_x)}=(N+1)\beta\rho^*_{\mathrm{Co}}t_{\mathrm{Co}}+2N\gamma AR^*_{\mathrm{Co/Ag}}. \tag{3.5}$$

Here N is the number of bilayers, β and γ are the spin-asymmetry scattering parameters for bulk Co and the Co/Ag interfaces, respectively, t_{Co} is the thickness of the individual Co layers, ρ^*_{Co} and $AR^*_{\mathrm{Co/Ag}}$ are suitably spin-averaged resistivity and specific interface resistance, respectively, A is the sample area as previously defined, and H_x represents either H_0 or H_P. The reader is referred to Ref. 22 for a more complete discussion of this equation and the parameters appearing in it. For our present discussion it is important to note that β, ρ^*_{Co}, γ, and $AR^*_{\mathrm{Co/Ag}}$ each will take on different

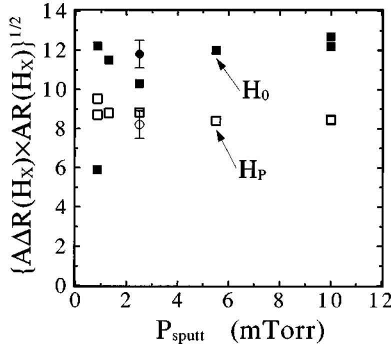

FIG. 9. The left-hand side of Eq. (3.5), determined using both the virgin state (H_0, filled points) and the peak state (H_P, open points) data, plotted vs sputtering pressure. The circular points give the predicted values for the plotted quantity based on parameters published in an earlier study of samples prepared at 2.5 mTorr with the error bars indicating the range allowed by the uncertainty in the values of those parameters (Ref. 22).

values for the H_0 and H_P states (since the level of antiparallel alignment for the magnetic layers differs in these two states). Equation (3.5) also suggests that if either β or γ (the two quantities of most fundamental interest to GMR) change as the structure of the samples changes, then we would expect the (measurement-derived) quantity on the left-hand side of Eq. (3.5) to depend on the sputtering pressure.

Figure 9 is a plot of the left-hand side of Eq. (3.5) vs sputtering pressure for both the virgin and peak state MR data. For both states, the plots are consistent with a zero slope (the observed negative slope for the peak state data differs from zero by only two standard deviations). Also plotted in Fig. 9 is the right-hand side of Eq. (3.5) calculated using the parameter values listed in Ref. 22 (obtained from a previous batch of samples all grown at 2.5 mTorr) for both the peak and virgin states. The agreement between this calculation and the results for the samples grown for this study is another indication of the overall reproducibility of samples used in these CPP studies. In computing this predicted value for the peak state CPP-MR, the two terms on the right-hand side of Eq. (3.5) have values of 0.8 and 7.4 fΩ m^2, respectively, which indicates that the spin-dependent scattering is predominantly (90%) at the interfaces in these samples. A similar dominance by the interfacial term is seen in the predicted value for the virgin state as well.

Since the right-hand side of Eq. (3.5) combines the spin-asymmetry parameters β and γ with the corresponding spin-averaged specific resistances $\rho^*_{\mathrm{Co}}t_{\mathrm{Co}}$ and $AR^*_{\mathrm{Co/Ag}}$, the separation of spin-dependent from spin-independent scattering accomplished by this equation is somewhat obscured. A simple rearrangement of the equation makes this feature more clear,

$$\sqrt{A\Delta R(H_x)\times AR(H_x)}=(N+1)\left(\frac{\rho^{\downarrow}-\rho^{\uparrow}}{4}\right)t_{\mathrm{Co}}+2N\left(\frac{AR^{\downarrow}_{\mathrm{Co/Ag}}-AR^{\uparrow}_{\mathrm{Co/Ag}}}{4}\right). \tag{3.6}$$

In obtaining Eq. (3.6) we have used the identities $\rho^{\downarrow(\uparrow)}_{\mathrm{Co}}=2\rho^*_{\mathrm{Co}}[1+(-)\beta]$ and $AR^{\downarrow(\uparrow)}_{\mathrm{Co/Ag}}=2AR^*_{\mathrm{Co/Ag}}[1+(-)\gamma]$, where $\downarrow$ ($\uparrow$) refers to a spin antiparallel (parallel) to the local magnetization. In this form one sees that a plot of the left-hand side vs sputtering pressure is a direct indication of how this deposition parameter influences the spin asymmetry of the scattering. Equation (3.6) explicitly shows that if disorder simply adds additional scattering that impacts both spin channels equally, such disorder will not change the left-hand-side quantity. Conversely, if changing the sample structure has a different impact on the majority and minority spins, then this should show up as a finite slope in a plot such as Fig. 9.

While it is possible that the negligible slope observed in Fig. 9 could arise from an accidental cancellation of competing trends for the antiparallel fraction in the H_P (or H_0) state and the difference $AR^{\uparrow}_{\mathrm{Co/Ag}}-AR^{\downarrow}_{\mathrm{Co/Ag}}$, it is much more probable that the disorder introduced at higher pressures simply increases the scattering in both the up and down spin channels [demonstrated by the increase in $AR(H_S)$ with pressure seen in Fig. 8] without affecting their difference. A similar cancellation between competing trends in the bulk and interfacial contributions is also possible but even more unlikely given the relative size of the contributions from these two terms. Although the observed slope for the peak state data is not inconsistent with this view, it is large enough to suggest that further investigation of this system with a study in which the interface structure and the antiparallel fraction are more directly controlled may be worthwhile.

It was pointed out in the Introduction of this paper that the sensitivity of the spin-dependent scattering to the details of interfacial structure is one of the outstanding unanswered questions in the GMR effect. Two competing ideas have recently been put forward on this question. For Fe/Cr multilayers, Beliën *et al.*[5] have suggested that step edges may enhance the GMR while interdiffusion and short-range roughness may reduce the effect. On the other hand, a recent calculation by Zhang and Levy indicates that simple intermixing at an interface can actually enhance spin-dependent scattering.[35] The present study finds no correlation between increased interfacial disorder (which in our case probably includes both topographic and chemical disorder) and spin-dependent scattering. Moreover, the spatial frequencies needed to distinguish directly between simple intermixing and a large concentration of step edges are beyond those available to low-angle off-specular x-ray scattering. Thus, the current work is not able to distinguish between these competing ideas regarding the effect of chemical disorder on spin-dependent scattering. This work does indicate that the Co/Ag system is an attractive one for further investigation of the connection between interfacial structure and magnetotransport, while it also displays the unique features that the CPP geometry brings to such a quest. The present results also emphasize the important role that the current-voltage contact layer can play in determining the structure and properties of multilayers when performing CPP measurements. This feature must be taken into account in future studies using the CPP geometry to relate structural changes to the spin-dependent scattering in GMR systems.

IV. CONCLUSION

Like other systems investigated previously, Co/Ag multilayers are seen to exhibit film growth that leads to rougher

interfaces at higher sputtering pressures. The crystalline coherence (as measured by the width of high-angle diffraction peaks) decreases monotonically with increasing pressure, but the structural order in the multilayers (as measured by the residual resistivity ratio and the roughness that is correlated from one interface to the next) exhibits a shallow maximum near a sputtering pressure of 2.5 mTorr. It has also been observed that the Nb layers used to make electrical contact in the CPP-MR measurements influence both the structure and magnetic properties of the multilayers being measured. The magnetic properties of the rather disordered multilayers produced at high sputtering pressures are altered by these Nb layers through thermal stress-induced changes to the multilayer's coercive field. The lower Nb contact layer is quite rough. This imposes a significant amount of vertically correlated roughness on the interfaces of the multilayer, and also has an impact on the growth of the film (seen in the crystalline coherence length). The dominant variation of the GMR ratio with sputtering pressure is an overall decrease in the effect, and for the ''peak'' state this decrease is found to come in roughly equal measure from an increase in the saturation resistance and a decrease in the field-dependent resistance. Unlike previous studies investigating the connection between interfacial structure and GMR using the CIP geometry, the present CPP study is able to conclude that this decrease in the MR is likely due primarily to an increase in spin-independent scattering rather than a change in the spin-dependent scattering at the interfaces in the samples.

ACKNOWLEDGMENTS

This work was supported by the NSF through Grant Nos. DMR94-623795, DMR94-00417 (MSU), DMR93-14018 (IU), MSU CFMR, MSU CSM, and Ford Research Laboratory. The authors would also like to acknowledge J. Bass for many fruitful discussions on this subject and comments on the manuscript.

[1] M. N. Baibich, J. M. Broto, A. Fert, F. Nguyen Van Dau, F. Petroff, P. Etienne, G. Creuzet, A. Friederich, and J. Chazelas, Phys. Rev. Lett. **61**, 2472 (1988).

[2] S. S. P. Parkin, N. More, and K. P. Roche, Phys. Rev. Lett. **64**, 2304 (1990).

[3] R. E. Camley and J. Barnas, Phys. Rev. Lett. **63**, 664 (1989).

[4] S. S. P. Parkin and B. R. York, Appl. Phys. Lett. **62**, 1842 (1993).

[5] P. Beliën, R. Schad, C. D. Potter, G. Verbanck, V. V. Moshchalkov, and Y. Bruynseraede, Phys. Rev. B **50**, 9957 (1994).

[6] T. Thomson, P. C. Riedi, and D. Grieg, Phys. Rev. B **50**, 10 319 (1994).

[7] E. E. Fullerton, D. M. Kelly, J. Guimpel, I. K. Schuller, and Y. Bruynseraede, Phys. Rev. Lett. **68**, 859 (1992).

[8] S. S. P. Parkin, Phys. Rev. Lett. **71**, 1641 (1993).

[9] M. Suzuki and Y. Taga, Phys. Rev. B **52**, 361 (1995).

[10] M. J. Hall *et al.*, J. Phys.: Condens. Matter **4**, L495 (1992).

[11] G. Tosin, L. F. Schelp, M. Carara, J. E. Schmidt, A. A. Gomes, and M. N. Baibich, J. Magn. Magn. Mater. **121**, 399 (1993).

[12] N. M. Rensing, A. P. Payne, and B. M. Clemens, J. Magn. Magn. Mater. **121**, 436 (1993).

[13] F. Petroff, A. Barthélémy, A. Hamzic, A. Fert, P. Etienne, S. Lequien, and G. Creuzet, J. Magn. Magn. Mater. **93**, 95 (1991).

[14] Y. Saito, K. Inomata, K. Yusu, A. Goto, and H. Yasuoka, Phys. Rev. B **52**, 6500 (1995).

[15] D. E. Savage, N. Schimke, Y.-H. Phang, and M. G. Lagally, J. Appl. Phys. **71**, 3283 (1992).

[16] K. Le Dang, P. Veillet, H. He, F. J. Lamelas, C. H. Lee, and R. Clarke, Phys. Rev. B **41**, 12 902 (1990).

[17] E. A. M. van Alphen, P. A. A. van der Heijden, and W. J. M. de Jong, J. Appl. Phys. **76**, 6607 (1994).

[18] C. Mény, P. Panissod, and R. Loloee, Phys. Rev. B **45**, 12 269 (1992).

[19] E. A. M. van Alphen, P. A. A. van der Heijden, and W. J. M. de Jong, J. Magn. Magn. Mater. **140-144**, 609 (1995).

[20] M. A. Parker, T. L. Hylton, K. R. Coffey, and J. K. Howard, J. Appl. Phys. **75**, 6382 (1994).

[21] J. M. Slaughter, W. P. Pratt, Jr., and P. A. Schroeder, Rev. Sci. Instrum. **60**, 127 (1989).

[22] S.-F. Lee, Q. Yang, P. Holody, R. Loloee, J. H. Hetherington, S. Mahmood, B. Ikegani, K. Vigen, L. L. Henry, W. P. Pratt, Jr., P. A. Schroeder, and J. Bass, Phys. Rev. B **52**, 15 426 (1995).

[23] W. P. Pratt, Jr., S.-F. Lee, J. M. Slaughter, R. Loloee, P. A. Schroeder, and J. Bass, Phys. Rev. Lett. **66**, 3060 (1991).

[24] J. B. Kortright, J. Appl. Phys. **70**, 3620 (1991).

[25] H. P. Klug and L. E. Alexander, *X-ray Diffraction Procedures for Polycrystalline and Amorphous Materials*, 2nd ed. (Wiley, New York, 1974).

[26] See for example equation (9-60) of Klug and Alexander (Ref. 25). We use $K=0.9$ for the constant of order unity in this equation.

[27] G. Palasantzas and J. Krim, Phys. Rev. B **48**, 2873 (1993).

[28] S. Dietrich and A. Haase, Phys. Rep. **260**, 1 (1995).

[29] M. Tolan, G. Vacca, S. K. Sinha, Z. Li, M. H. Rafailovich, J. Sokolov, H. Lorenz, and J. P. Kotthaus, Appl. Phys. Lett. **68**, 191 (1996).

[30] V. Holý and T. Baumbach, Phys. Rev. B **49**, 10 668 (1994).

[31] Y. Yoneda, Phys. Rev. **131**, 2010 (1963).

[32] M. Kopecký, J. Appl. Phys. **77**, 2380 (1995).

[33] S. K. Sinha, E. B. Sirota, S. Garoff, and H. B. Stanley, Phys. Rev. B **38**, 2297 (1988).

[34] W. P. Pratt, Jr., Q. Yang, P. Holody, W.-C. Chiang, P. A. Schroeder, and J. Bass, J. Appl. Phys. **79**, 5811 (1996), and references therein.

[35] S. Zhang and P. M. Levy, Phys. Rev. Lett. **77**, 916 (1996).